Available online at www.sciencedirect.com
SCIENCE DIRECT®
International Journal of Heat and Mass Transfer 48 (2005) 3833–3854
International Journal of HEAT and MASS TRANSFER
www.elsevier.com/locate/ijhmt

Laminar natural convection in an inclined complicated cavity with spatially variable wall temperature

Amaresh Dalal [1], Manab Kumar Das *

Department of Mechanical Engineering, Indian Institute of Technology Guwahati, Guwahati 781 039, India

Received 3 November 2003; received in revised form 22 June 2004

Abstract

Natural convection in two-dimensional enclosure with three flat and one wavy walls is numerically investigated. One wall is having a sinusoidal temperature profile. Other three walls including the wavy wall are maintained at constant cold temperature. This problem is solved by SIMPLE algorithm with deferred QUICK scheme in curvilinear co-ordinates. The tests were carried out for different inclination angles, amplitudes and Rayleigh numbers while the Prandtl number was kept constant. The geometrical configurations considered were namely one-, two- and three-undulations.

The results obtained show that the angle of inclination affects the flow and heat transfer rate in the cavity. With increase in amplitude, the average Nusselt number on the wavy wall is appreciably high at low Rayleigh number. Increasing the number of undulations beyond two is not beneficial. The trend of local Nusselt number is wavy.

Keywords: Natural convection; Wavy wall; Square cavity; Spatially variable temperature; Numerical simulation

1. Introduction

The natural convection process has developed considerable importance because of its relevance to heat transfer in many engineering applications. These are cooling of electronic components, heating and cooling of rooms, solar heaters, crystal growth, glass melting to name a few of them. Since the velocity and the temperature equations are coupled due to the buoyancy force, the study of natural convection is very complex.

When in an enclosure, the two vertical walls are differentially heated and the horizontal top and bottom walls are maintained under adiabatic conditions, a fluid flow is developed because of the horizontal temperature difference ΔT_H. The density difference gradient (i.e., temperature difference gradient) is horizontal and the gravity vector acts perpendicularly. These two vectors act normal to each other and the direction of the circulation depends upon their orientation. However, the situation becomes more complex when these two vectors are parallel to each other. When the bottom wall is heated and the top wall is cooled, i.e., there is a vertical temperature difference ΔT_V, the density increases from bottom to top. These two vectors (i.e., density gradient and gravity) are parallel and opposite to each other. In this case

* Corresponding author. Tel.: +91 361 2582655; fax: +91 361 2690762.
E-mail addresses: d_amaresh@yahoo.com (A. Dalal), manab@iitg.ernet.in (M.K. Das).
[1] Present address: Department of Mechanical Engineering, Indian Institute of Technology—Kanpur, Kanpur 208016, India.

0017-9310/$ - see front matter © 2005 Elsevier Ltd. All rights reserved.
doi:10.1016/j.ijheatmasstransfer.2004.07.051

Nomenclature

g	gravitational acceleration
H	height of the enclosure
J	Jacobian
Nu	Nusselt number
Nu_{av}	average Nusselt number $= \frac{1}{s}\int_0^s Nu_l \, ds$
Nu_{max}	the maximum value of local Nusselt number on the boundary at $x = 0$
Nu_{min}	the minimum value of local Nusselt number on the boundary at $x = 0$
p	dimensionless pressure
Pr	Prandtl number
P, Q	grid control functions
Ra	Rayleigh number $= g\beta\Delta T H^3/(v\alpha)$
T	dimensionless temperature
ΔT	differential temperature, dimensionless
u, v	dimensionless velocity components in x and y direction
U, V	dimensionless contravariant velocity components in ξ and η direction
u_{max}	the maximum horizontal velocity on the vertical mid plane of the cavity
v_{max}	the maximum vertical velocity on the horizontal mid plane of the cavity
x, y	dimensionless Cartesian coordinates

Greek symbols

α	thermal diffusivity
ϕ	inclination angle
ϑ	general variable representing u, v and T
ξ, η	dimensionless curvilinear coordinates
λ	wave amplitude

Subscripts

c, h	cold wall and hot wall
H	horizontal
V	vertical
w	wall
x, y	derivative relative to x, y, respectively
ξ, η	derivative relative to ξ, η, respectively

Superscript

*	dimensional form

the circulation will start after a critical Rayleigh number is reached (Bénard convection). In the case of top wall being heated and the bottom wall being cooled, the density increases from top to bottom. The two vectors are parallel and acting in the same direction. The fluid is thermally stratified and there will be no circulation in this case.

In an enclosure, if the four walls are either heated or cooled, there will exist a ΔT_H and ΔT_V. By choosing a proper ΔT_H and ΔT_V, it is possible to generate two circulations of opposite direction inside the enclosure. This method can be used to control the fluid circulation inside the enclosure. The situations will change in the case of tilted enclosure.

The natural convection process inside a rectangular enclosure has been studied extensively for the last four decades. Ostrach [1] has given a review of the history and developments of such heat transfer process with the inception of natural convection as a research topic. The heat transfer process is dominated by conduction when the Rayleigh number is low. With the increase of Rayleigh number, thermal boundary layer forms adjacent to the wall and a core region is formed. The heat transfer is then dominated by convection. It is the interaction of this core region with the boundary layer that makes the understanding of the heat transfer process very complex. Depending upon the aspect ratio (height/width), the fluid flow pattern will change with the variation in Rayleigh number.

Two-dimensional experimental studies or numerical solutions inside a differentially heated rectangular enclosure tilted at different angles have been carried out under various conditions. During the last decade, the subject of natural convection in inclined cavities has been extended by additional variations. Research has been done on the influence of change in geometry and on changes in the boundary conditions.

An enclosure with corrugated bottom surface maintaining a uniform heat flux and flat isothermal cooled top surface and side walls adiabatic was studied by Noorshahi et al. [2]. The results show that the pseudo-conduction region is increased with increase of wave amplitude. The natural convection heat transfer in a two-dimensional rectangular enclosure fitted with a periodic array of hot roughness elements at the bottom has been investigated numerically [3]. Bottom surface is heated and the right vertical wall is cooled and the other walls are adiabatic. Increase in heat transfer is obtained when the roughness element phase shift is equal to half its period. The increment in heat transfer is found to be more significant for enclosures with higher values of roughness element amplitude.

Yao [4] has studied theoretically the natural convection along a vertical wavy surface. He found that the local heat transfer rate is smaller than that of the flat plate case and decreases with increase of the wave amplitude. The average Nusselt number also shows the same trend. Adjlout et al. [5] reported a numerical study of the effect

of a hot wavy wall in an inclined differentially heated square cavity. Tests were performed for different inclination angles, amplitudes and Rayleigh numbers for one- and three-undulations. The trend of the local heat transfer is wavy. The mean Nusselt number decreases comparing the square cavity.

The effect of non-uniform temperature distribution on an inclined three-dimensional enclosure has been studied by Chao et al. [6]. Bottom wall is maintained at a saw-toothed temperature distribution with different amplitude and orientation while top wall is isothermal and other faces are adiabatic. The circulation pattern did not change significantly with the temperature distributions. The Nusselt number does not change significantly with inclination. Chao et al. [7] in another study considered half of the bottom surface heated and the top surface cooled, while half of the bottom surface and other vertical surfaces were adiabatic. The observed and predicted patterns of circulation are found to be in good agreement. A numerical study of natural convection in an enclosure was investigated where the heated wall of the enclosure is divided into two higher and lower temperature regions and the temperature of the cold wall is maintained at a constant [8]. The results show that the local Nusselt number distribution varies drastically at the intersection of the higher and lower temperature regions, and the flow is strongly affected by the above two parameters.

Convective motion in a square cavity with linearly varying temperature imposed along the top surface has been investigated numerically by Shukla et al. [9]. The side and bottom walls of the rigid cavity are assumed to be insulated. For low Rayleigh number, a single convective cell is formed. With increase in Rayleigh number, flow and temperature fields become asymmetric. The temperature field is generally stratified with lower part of cavity relatively isothermal. Oosthuizen and Paul [10] considered an enclosure with side wall partially heated and top wall cooled. In another study, Oosthuizen [11] considered an enclosure with bottom surface heated and the top surface is inclined and maintained at uniform cold temperature. The temperature of the side walls varies in a prescribed way between the bottom and the top wall temperatures. The proposed system is found in crop drying applications such as corn and rice. The top surface inclination has been varied between 0° and 45°, aspect ratio 0.25 and 1 and Rayleigh number 10^3 and 10^7. The effect of changes in governing parameters on flow pattern and mean heat transfer rate to the upper surface has been studied. Heating from the top wall leads to thermal stratification. However, if the temperature imposed has a sinusoidal distribution, two cells counter rotating will be formed. This kind of heating is found in glass technology. In a study carried out by Sarris et al. [12], the top wall is periodically heated while the side walls and the bottom wall are adiabatic. This ensures that the top wall controls the flow. The thermal boundary layer is confined near the top wall. The values of maximum and minimum Nusselt number is shown to increase with increase of Rayleigh number.

From the above literature survey, the following observations are made. Though a large amount of literature is available on studies concerning rectangular and nonrectangular geometry, not much focus has been given on natural convection in enclosures with vertical wavy wall. It has been found that in most of the cases, the walls are differentially heated either in the horizontal or in the vertical directions. Problems concerning the simultaneous imposition of these two types of boundary conditions are rare in the literature. Again, it has been found that temporally varying boundary conditions (not mentioned here) are present in the literature, whereas spatially varying boundary conditions have not been given much importance.

In the present study, a natural convection problem has been solved in a square enclosure having three flat walls and the wavy vertical wall consisting of one-, two- and three-undulations of varying amplitudes. The two vertical walls and the bottom wall are maintained at a fixed lower temperature. The top wall is heated with sinusoidally varying temperature distribution in the space coordinate. Air has been taken as the working fluid ($Pr = 0.71$). The study has been conducted at different inclination of the enclosure from 0° to 360° in steps of 30°.

1.1. Problem specification

The problem considered is a two-dimensional heat transfer in a square cavity with wavy right vertical wall filled with viscous fluid. The upper wall temperature is considered to be spatially varying with sinusoidal temperature distribution, $T^*_w(x^*)$. The other three walls are considered to be of constant temperature, T^*_c. The temperature distribution on the top wall is as follows [12]:

$$T^*_w(x^*) = T^*_c + \frac{\Delta T^*}{2}\left(1 - \cos\left(\frac{2\pi x^*}{H}\right)\right), \tag{1}$$

where T^*_c is the minimum value of the imposed temperature distribution, ΔT^* is the temperature difference between the maximum and the minimum temperatures of the upper wall, and H is the length of the square enclosure. The above equation can be written in the dimensionless form (Eq. (4)) as follows and the dimensionless temperature distribution of the top wall is shown in Fig. 1:

$$T_w(x) = \tfrac{1}{2}(1 - \cos(2\pi x)). \tag{2}$$

The shape of the wavy vertical wall is taken as sinusoidal. The expression of the wavy wall is given by

$$f(y) = [1 - \lambda + \lambda(\cos 2\pi n y)], \tag{3}$$

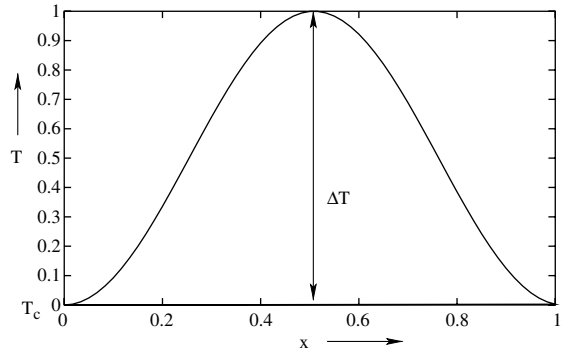

Fig. 1. Imposed temperature distribution (dimensionless) on the heated surface.

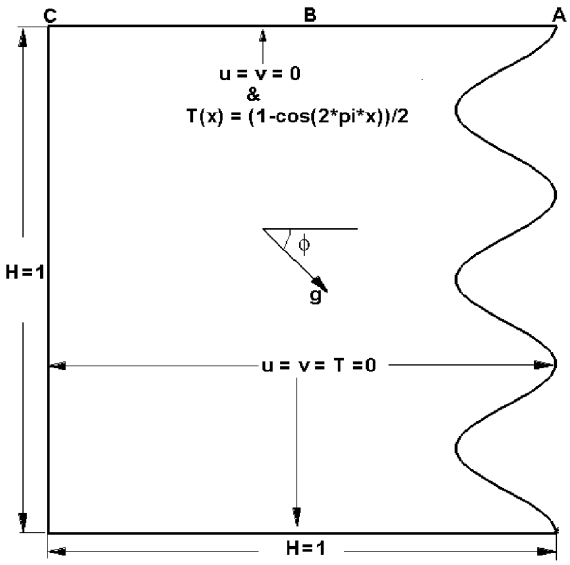

Fig. 2. Geometrical details of the cavity.

where n is the number of undulations and λ is the amplitude [5]. Three different cases with one-, two- and three-undulation are studied. The amplitude for all three cases have been varied from 0.01 to 0.10 in steps 0f 0.01. The Rayleigh number is varied from 10^0 to 10^6. Prandtl number is fixed to be 0.71. Fig. 2 shows the geometrical features of the cavity.

2. Governing equations and boundary conditions

Natural convection is governed by the differential equations expressing the conservation of mass, momentum, and energy. The present flow is considered steady, laminar, incompressible and two-dimensional. The viscous dissipation term in the energy equation is neglected. The momentum equations are simplified using Boussinesq approximation, in which all fluid properties are assumed constant except the density in its contribution to the buoyancy force. The governing equations and the boundary conditions are cast in dimensionless form using the following dimensionless variables:

$$x=\frac{x^*}{H},\quad y=\frac{y^*}{H},\qquad u=\frac{u^*H}{\alpha},\quad v=\frac{v^*H}{\alpha},\qquad p=\frac{p^*H^2}{\rho\alpha^2},\quad T=\frac{T^*-T_c^*}{\Delta T^*}. \tag{4}$$

Continuity equation:

$$\frac{\partial u}{\partial x}+\frac{\partial v}{\partial y}=0, \tag{5}$$

u-momentum equation:

$$\frac{\partial(u^2)}{\partial x}+\frac{\partial(uv)}{\partial y}=-\frac{\partial p}{\partial x}+Pr\left(\frac{\partial^2 u}{\partial x^2}+\frac{\partial^2 u}{\partial y^2}\right)-Ra\,Pr\,T\cos\phi, \tag{6}$$

v-momentum equation:

$$\frac{\partial(uv)}{\partial x}+\frac{\partial(v^2)}{\partial y}=-\frac{\partial p}{\partial y}+Pr\left(\frac{\partial^2 v}{\partial x^2}+\frac{\partial^2 v}{\partial y^2}\right)+Ra\,Pr\,T\sin\phi, \tag{7}$$

energy equation:

$$\frac{\partial(uT)}{\partial x}+\frac{\partial(vT)}{\partial y}=\frac{\partial^2 T}{\partial x^2}+\frac{\partial^2 T}{\partial y^2}. \tag{8}$$

In addition, the velocity and temperature boundary conditions, take the following form:

$$u=v=T=0 \quad \text{for } x=0,1 \text{ and } 0\leqslant y\leqslant 1, \tag{9a}$$

$$u=v=T=0 \quad \text{for } x=f(y)=[1-\lambda+\lambda(\cos 2\pi n y)] \text{ and } 0\leqslant y\leqslant 1, \tag{9b}$$

$$u=v=T=0 \quad \text{for } y=0 \text{ and } 0\leqslant x\leqslant 1, \tag{9c}$$

$$u=v=0 \text{ and } T=\tfrac{1}{2}(1-\cos(2\pi x)) \quad \text{for } y=1 \text{ and } 0\leqslant x\leqslant 1. \tag{9d}$$

2.1. Transformation of the governing equations

The governing equations transformed from the Cartesian system (x,y) to the boundary-fitted coordinate system (ξ,η) are given by [13,14].

Continuity equation

$$U_\xi+V_\eta=0, \tag{10}$$

Generalised momentum and energy equations

$$(U\vartheta)_\xi+(V\vartheta)_\eta=S(\xi,\eta)+\left\{\frac{\Gamma}{J}(\alpha\vartheta_\xi-\beta\vartheta_\eta)\right\}_\xi+\left\{\frac{\Gamma}{J}(-\beta\vartheta_\xi+\gamma\vartheta_\eta)\right\}_\eta, \tag{11}$$

where $\Gamma = Pr$ for the momentum equations and $\Gamma = 1$ for the energy equation. The source term $S(\xi,\eta)$ is given by

$$S(\xi,\eta) = -y_\eta p_\xi + y_\xi p_\eta \quad \text{for } \vartheta = u, \tag{12a}$$

$$S(\xi,\eta) = x_\eta p_\xi - x_\xi p_\eta + J\,Ra\,Pr\,T \quad \text{for } \vartheta = v, \tag{12b}$$

$$S(\xi,\eta) = 0 \quad \text{for } \vartheta = T. \tag{12c}$$

The relationships between the Cartesian and contravariant velocity components are

$$U = y_\eta u - x_\eta v, \quad V = x_\xi v - y_\xi u. \tag{13}$$

The boundary conditions given in Eq. (9) are Dirichlet type. The boundary conditions on the computational plane can be written as follows:

$$u = v = T = 0 \quad \text{for } \xi = 0, 1 \text{ and } 0 \leqslant \eta \leqslant 1, \tag{14a}$$

$$u = v = T = 0 \quad \text{for } \eta = 0 \text{ and } 0 \leqslant \xi \leqslant 1, \tag{14b}$$

$$u = v = 0 \text{ and } T = \tfrac{1}{2}(1 - \cos(2\pi x)) \quad \text{for } \eta = 1 \text{ and } 0 \leqslant \xi \leqslant 1. \tag{14c}$$

The heat transfer rate by convection in an enclosure is obtained from the Nusselt number calculation. The local Nusselt Nu_l numbers on the four walls are expressed as

$$\text{Top wall} \quad Nu_l = \frac{1}{J\sqrt{\gamma}}(\gamma T_\eta - \beta T_\xi), \tag{15a}$$

$$\text{Right wall} \quad Nu_l = \frac{1}{J\sqrt{\gamma}}(\alpha T_\xi - \beta T_\eta), \tag{15b}$$

$$\text{Bottom wall} \quad Nu_l = -\frac{1}{J\sqrt{\gamma}}(\gamma T_\eta - \beta T_\xi), \tag{15c}$$

$$\text{Left wall} \quad Nu_l = -\frac{1}{J\sqrt{\gamma}}(\alpha T_\xi - \beta T_\eta). \tag{15d}$$

The average Nusselt number is the average of local Nusselt number along a wall and is defined by the following equation:

$$Nu_{av} = \frac{1}{s}\int_0^s Nu_l \, ds. \tag{16}$$

2.2. Grid generation

Numerical grid generation has now become a fairly common tool for use in the numerical solution of partial differential equations on arbitrarily shaped regions. The coordinate transformation technique advanced by Thompson et al. [15] is used for the solution of problems over complex geometries. The transformation is obtained from the solution of partial differential equations on the regular computational domain. Mapping is done to convert the regions having irregular shape (physical domain) into the computational domain where the geometry becomes regular (computational domain) with a suitable transformation. A curvilinear mesh is generated over the physical domain such that one member of each family of curvilinear coordinate lines is coincident with the boundary contour of the physical domain [16]. The Navier–Stokes equations are then solved on the transformed plane and the solution is back-transformed to the physical plane. The transformation is as follows:

$$\xi \equiv \xi(x,y), \quad \eta \equiv \eta(x,y), \tag{17}$$

and the inverse transformation is given by

$$x \equiv x(\xi,\eta), \quad y \equiv y(\xi,\eta). \tag{18}$$

The mapping to the body fitted coordinate system is constructed by specifying the desired points (x,y) on the boundary of the physical domain. The distribution of points on the interior is determined by solving a system of Poisson equations:

$$\xi_{xx} + \xi_{yy} = P(\xi,\eta), \tag{19}$$

$$\eta_{xx} + \eta_{yy} = Q(\xi,\eta). \tag{20}$$

Eqs. (19) and (20) are then transformed to computational space by interchanging the roles of the independent and dependent variables. This yields a system of two equations of the form

$$\delta x_{\xi\xi} - 2\beta x_{\xi\eta} + \gamma x_{\eta\eta} + J^2(Px_\xi + Qx_\eta) = 0, \tag{21}$$

$$\delta y_{\xi\xi} - 2\beta y_{\xi\eta} + \gamma y_{\eta\eta} + J^2(Py_\xi + Qy_\eta) = 0, \tag{22}$$

where the geometric coefficients δ, β, γ and the Jacobian are given by

$$\delta = x_\eta^2 + y_\eta^2, \tag{23a}$$

$$\beta = x_\xi x_\eta + y_\xi y_\eta, \tag{23b}$$

$$\gamma = x_\xi^2 + y_\xi^2, \tag{23c}$$

$$J = x_\xi y_\eta - x_\eta y_\xi, \tag{23d}$$

P and Q are functions that provide control of the mesh concentration. The values of P and Q have to be chosen depending on the clustering of the grid required for the problem in hand. The transformed Eqs. (21) and (22) are discretized over the computational plane using second-order differencing and then solved numerically. The coefficients in Eq. (23) are computed at each grid point. For the present study, the grid used are shown in Fig. 3(a)–(c).

3. Numerical procedure

The governing equations are discretized on a structured grid. The velocity components and the scalar variables (pressure, temperature) are located on the grid in a staggered manner. The governing equations are solved numerically by finite volume method. The semi implicit method for pressure linked equation (SIMPLE) [17] is used to couple momentum and continuity equations.

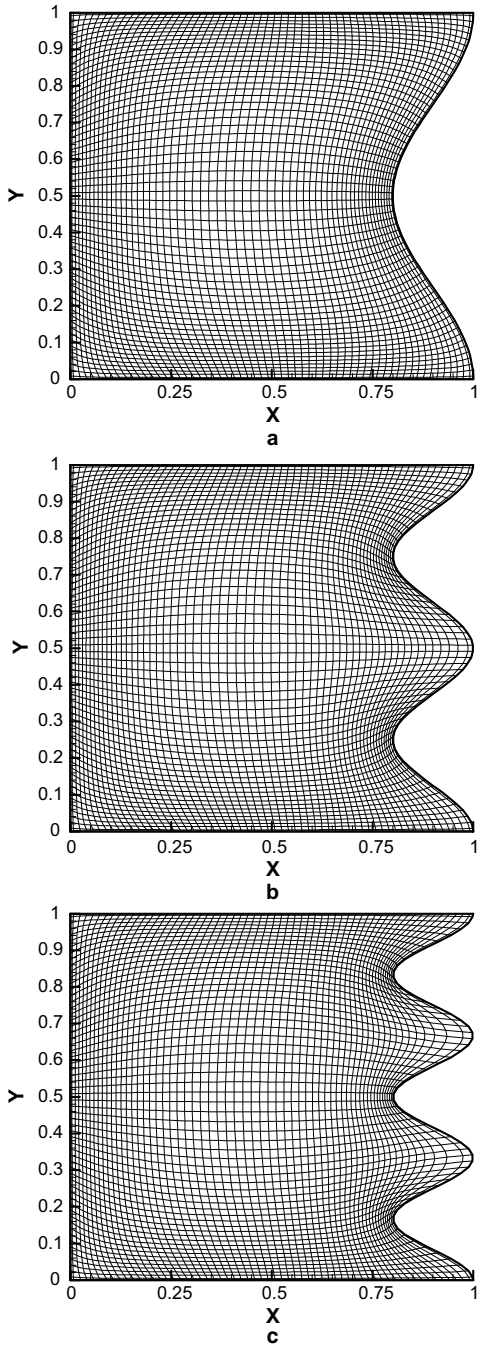

Fig. 3. Mesh distribution in the cavity for one-, two- and three-undulations.

The deferred QUICK scheme of Hayase et al. [18] is employed to minimize numerical diffusion for the convective terms for both the momentum equations and energy equation. The central difference scheme of Patankar [17] is employed near the boundary points for the convective terms. The solution of the discretized momentum and pressure correction equation is obtained by line-by-line method [17]. The pseudo-transient approach is followed for the numerical solution as it is useful for situation in which the governing equations give rise to stability problems, e.g., buoyant flows [19]. Under-relaxation factor for pressure with values of 0.01 was used.

The iterative procedure is initiated by the solution of energy equation followed by momentum equations and is continued until convergence is achieved. Euclidean norm of the residual is taken as convergence criteria for each dependent variable in the entire flow field [20]. The mass balance for global convergence was taken as 10^{-8}. The calculations were performed on Pentium III, 128 RAM machine.

3.1. Grid independence study of the problem concerned

The grid independence test is performed using successively sized grids, 21×21, 41×41, 61×61 and 81×81 for $Ra = 10^4$ and 10^6, $\lambda = 0.05$ and $\phi = 90°$. The distribution of local Nusselt number at wavy wall for one- and three-undulations are shown in Fig. 4(a) and (b), respectively, when $Ra = 10^4$ whereas for $Ra = 10^6$, they are shown in Fig. 4(c) and (d), respectively. It is observed that the curves overlap with each other for 61×61 and 81×81. So a grid number of 61×61 is chosen for further computation.

3.2. Code validation

The present code is validated for natural convection heat transfer by comparing the results of a buoyancy driven laminar heat transfer in a square cavity with differentially heated side walls. The left wall was kept hot while the right wall was cooled. The top and bottom walls are insulated. In the present work numerical predictions, using the developed algorithm, have been obtained for Rayleigh numbers between 10^3 and 10^5 on elliptic mesh with 61×61 grid points.

Table 1 compares the results with those by de Vahl Davis [21], Markatos and Perikleous [22] and Hadjisophocleous et al. [23]. The results are in very good agreement with the benchmark solution, especially for the lower Rayleigh numbers. At higher Rayleigh numbers more points are needed close to the vertical walls for an accurate evaluation of the wall temperature gradient [23].

4. Results and discussion

A parametric study was carried out to determine the influence of inclination angle (ϕ), Ra, amplitude (λ) and number of undulations on the flow field of air. Inclina-

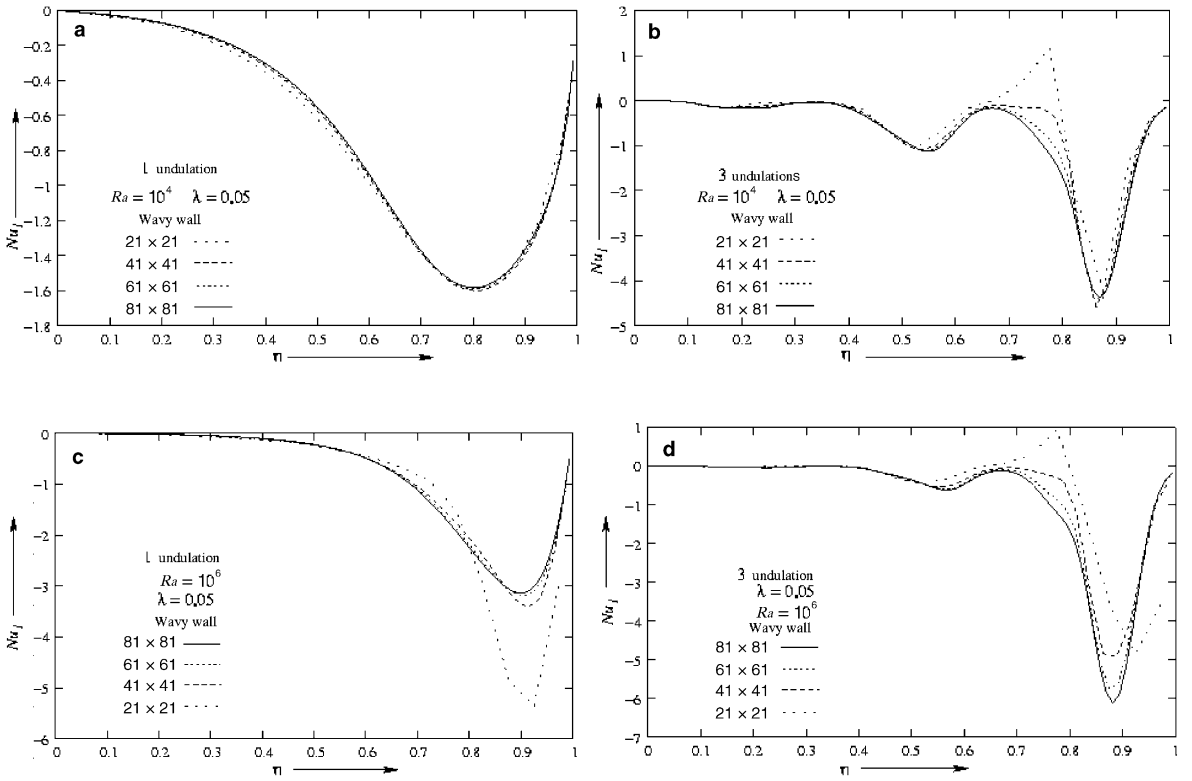

Fig. 4. Grid independence test: Comparison of local Nu on the right wall. (a) For $Ra = 10^4$, one-undulation, wavy wall, $\phi = 90°$; (b) for $Ra = 10^4$, three-undulations, wavy wall, $\phi = 90°$; (c) for $Ra = 10^6$, one-undulation, wavy wall, $\phi = 90°$ and (d) For $Ra = 10^6$, three-undulations, wavy wall, $\phi = 90°$.

tion angle (ϕ) was considered in the range of 0–360° in steps of 30° to obtain the inclination. The Ra was varied between 10^0 and 10^6 to cover a large range. The influence of the amplitude (λ) was examined for the values in between 0.01 and 0.1. All these cases were computed for one-, two- and three-undulations.

4.1. Streamtraces and isotherms

Figs. 5–10 show the streamtraces and isotherms for $Ra = 10^5$ and $\lambda = 0.05$. The action of the gravity vector is shown by arrow. For $\phi = 0°$ (Fig. 5(a)), there is mainly one cell encompassing the complete domain with an extremely small one at one corner. The main flow is observed to be in the counter clockwise direction because the sinusoidally varying temperature is on the right side of the gravity vector. Similar trend is obtained for two wave and three waves cases (Fig. 7(a) and Fig. 9(a)). The inner streamtraces are pushed towards the corner which is depicted as C in Fig. 2. Because of the sinusoidally varying temperature distribution, the location A and C are cold and B is hot (Fig. 2). The circulation is setting in because the hot fluid B is raising up displacing cold fluid at C and thus a counter clockwise flow is occurring. For $\phi = 180°$, the heated wall is on the left hand side of the gravity vector and a clockwise rotation is taking place.

In both the cases, the inner rotating cell is cusped towards the end of the heated wall opposite to the gravity vector. Unlike the case of a differentially heated side walls and other two insulated horizontal walls [21], for $Ra = 10^5$, only one rotating cell inside the core is observed for these two cases.

For $\phi = 90°$ (Fig. 5(d), Fig. 7(d) and Fig. 9(d)), the conditions are somewhat similar to the problem studied by Sarris et al. [12]. In their problem, the top wall had a sinusoidally varying temperature and other three walls are adiabatic. The gravity vector was acting from top to bottom wall. Since the temperature is varying on the top wall, we are getting a ΔT_V which is varying in the x-direction. So in spite of ΔT_V parallel to the gravity vector and the top surface is hot, a circulation is set in instead of a thermally stratified medium. Two counter rotating cells (one counter clock wise and another clock wise) are formed. Here also the inner of the two rotating cells are directed towards the end points of the heated wall. When the direction of the gravity vector is reversed, i.e., $\phi = 270°$ (Fig. 5(j), Fig. 7(j) and Fig. 9(j)),

Table 1
Comparison of solutions for natural convection in an enclosed cavity

	a	*b*	*c*	*d*	$\frac{a-d}{a} \times 100$
(a) $Ra = 10^3$					
u_{max}	3.649	3.544	3.544	3.660	−0.3015
y	0.813	0.832	0.814	0.725	
v_{max}	3.697	3.593	3.586	3.706	−0.2434
x	0.178	0.168	0.186	0.258	
Nu_{max}	1.505	1.496	1.540	1.491	0.9302
y	0.092	0.0825	0.142	0.125	
Nu_{min}	0.692	0.720	0.727	0.670	0.3179
y	1.0	0.9925	0.991	0.991	
(b) $Ra = 10^4$					
u_{max}	16.178	16.18	15.995	16.292	−0.7047
y	0.823	0.832	0.814	0.742	
v_{max}	19.617	19.44	18.894	19.744	0.6474
x	0.119	0.113	0.103	0.192	
Nu_{max}	3.528	3.482	3.84	3.5050	−0.7936
y	0.143	0.1425	0.141	0.158	
Nu_{min}	0.586	0.643	0.670	0.569	−2.90
y	1.0	0.9925	0.991	0.991	
(c) $Ra = 10^5$					
u_{max}	34.73	35.73	37.144	34.992	−0.7544
y	0.855	0.857	0.855	0.775	
v_{max}	68.59	69.08	68.91	68.79	−0.2916
x	0.066	0.067	0.061	0.125	
Nu_{max}	7.117	7.626	8.93	7.582	−6.534
y	0.081	0.0825	0.080	0.091	
Nu_{min}	0.729	0.824	1.01	0.701	3.841
y	1.0	0.9925	1.0	0.991	
(d) $Ra = 10^6$					
u_{max}	64.63	68.81	66.42	64.99	−0.5605
y	0.850	0.872	0.897	0.775	
v_{max}	217.36	221.8	226.4	221.27	−1.7988
x	0.0379	0.0375	0.0206	0.075	
Nu_{max}	17.925	17.872	21.41	20.04	−11.7992
y	0.0378	0.0375	0.030	0.025	
Nu_{min}	0.989	1.232	1.58	0.916	−7.3811
y	1.0	0.9925	1.0	0.991	

a: solution of de Vahl Davis [21]; *b*: solution of Markatos and Perikleous [22]; *c*: solution of Hadjisophocleous et al. [23]; *d*: present solution on 61×61 grid.

a similar trend is noticed. There is a formation of two counter rotating vortices. But the direction of rotation is interchanged.

The origin of this phenomenon is due to the sinusoidally varying boundary temperature and the orientation angle (ϕ). It can be observed that small vortices are formed next to the wavy walls, $\phi = 30°$ (Fig. 5(b), Fig. 7(b) and Fig. 9(b)) which grow in larger size for $\phi = 60°$ (Fig. 5(c), Fig. 7(c) and Fig. 9(c)) and coalesce to form a rotating cell when $\phi = 90°$ (Fig. 5(d), Fig. 7(d) and Fig. 9(d)). With further increase in angle of rotation $\phi = 120°$, this cell grows bigger in size and squeezes the other cell (Fig. 5(e), Fig. 7(e) and Fig. 9(e)). The point to be noted is that, the core of the other cell breaks down in two small cells. For $\phi = 150°$, this cell has grown in such a size that the other cell has disappeared (Fig. 5(f), Fig. 7(f) and Fig. 9(f)) and for $\phi = 180°$, this cell completely covers the whole domain (Fig. 5(g), Fig. 7(g) and Fig. 9(g)).

Same sequence of phenomena is observed at $\phi = 210°$ (Fig. 5(h), Fig. 7(h) and Fig. 9(h)), 240° (Fig. 5(i), Fig. 7(i) and Fig. 9(i)), 270° (Fig. 5(j), Fig. 7(j) and Fig. 9(j)), 300° (Fig. 5(k), Fig. 7(k) and Fig. 9(k)) and 330° (Fig. 5(l), Fig. 7(l) and Fig. 9(l)). So, it can be said that periodically vortices are formed from the wavy wall and finally disappearing to the opposite flat wall for various angle of rotation.

For high Ra (10^5 and above) advection is the mode of heat transfer neat the heated wall [12]. The similar feature is noted in the present problem for $\phi = 90°$ (Fig. 6(d), Fig. 8(d) and Fig. 10(d)). The isotherms concentrate near the heated wall and heat transfer is high. However, half of the domain is very cold (T below 0.05) signifying the heat is unable to penetrate into this region. For $\phi = 270°$ (Fig. 6(j), Fig. 8(j) and Fig. 10(j)), heat is advected throughout the region resulting in a distribution of the isotherms. We do not have a central core region in general.

The effect of angle of orientation on the isotherms and convection are given in the following plots. For $\phi = 0°$ (Fig. 6(a), Fig. 8(a) and Fig. 10(a)), the isotherm spread well over the domain. They gradually shift towards the heated wall for $\phi = 30°$ (Fig. 6(b), Fig. 8(b) and Fig. 10(b)) and $\phi = 60°$ (Fig. 6(c), Fig. 8(c) and Fig. 10(c)). The opposite phenomena occur when ϕ is further increased. The isotherms spread gradually from the top wall for $\phi = 120°$ (Fig. 6(e), Fig. 8(e) and Fig. 10(e)) and $\phi = 150°$ (Fig. 6(f), Fig. 8(f) and Fig. 10(f)). For these cases, the isotherms are densely packed near the wavy wall. The isotherms are well distributed for $\phi = 210°$ (Fig. 6(h), Fig. 8(h) and Fig. 10(h)) and $\phi = 240°$ (Fig. 6(i), Fig. 8(i) and Fig. 10(i)). For $\phi = 300°$ (Fig. 6(k), Fig. 8(k) and Fig. 10(k)) and $\phi = 330°$ (Fig. 6(l), Fig. 8(l) and Fig. 10(l)) the isotherms are closer to each other near the opposite wavy wall.

4.2. Temperature profile

The temperature profile at $x = 0.5$ has been plotted for two-undulations, $Ra = 10^5$ and amplitude = 0.05 with ϕ as parameter (Fig. 11(a)–(c)). With the increase in ϕ from 0° to 90° (Fig. 11(a)) it is observed that the convection effects are diminishing at the lower half and a boundary layer profile emerges [12]. With further increase in ϕ from 120° to 210° (Fig. 11(b)), the boundary layer profile gives way to a convection dominated profile. When ϕ is in the range of 240–330°, convection effects are predominant. Fig. 11(d) is the plot of T with Ra as parameter. With an increase in Ra, the boundary

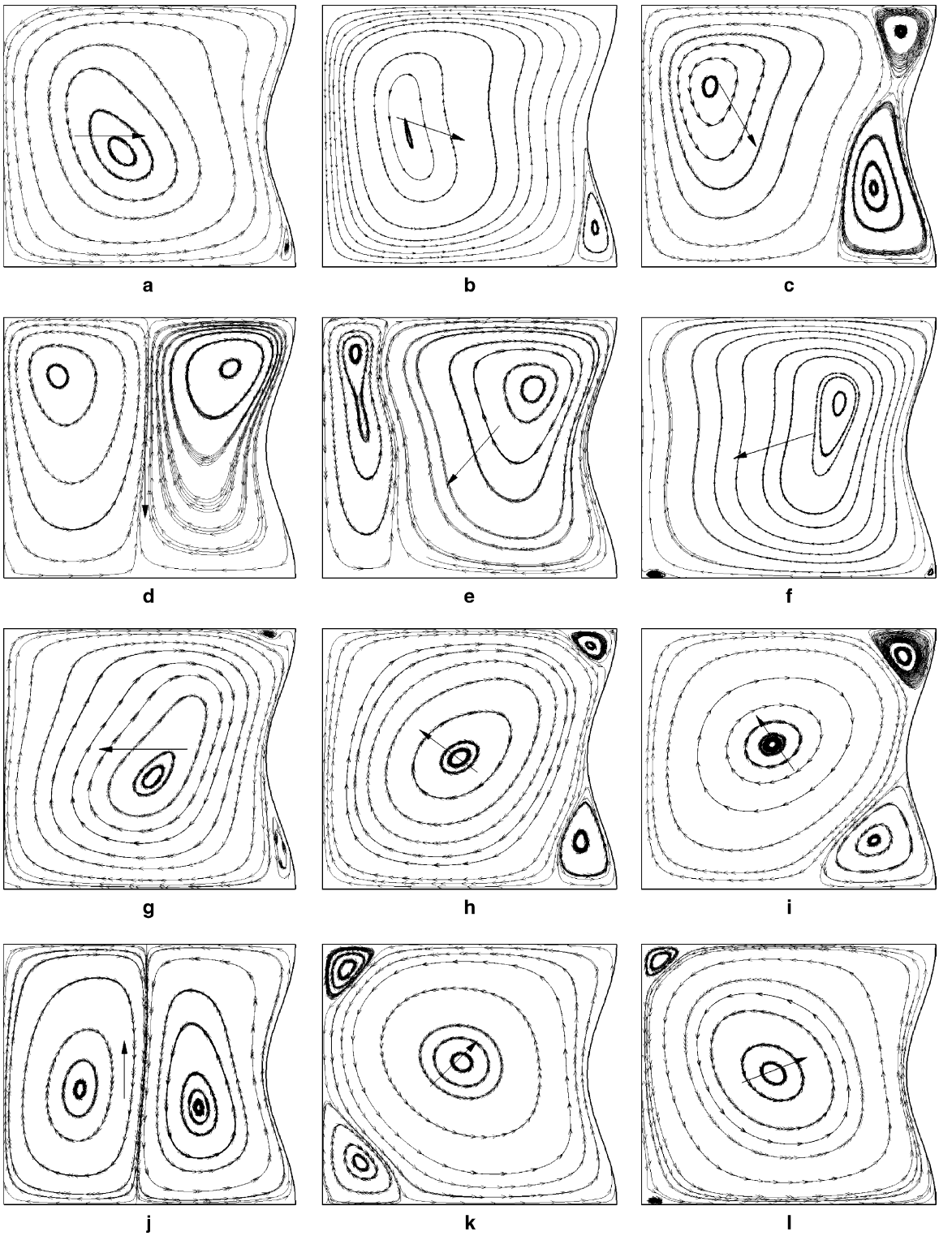

Fig. 5. Streamtraces for $Ra = 10^5$, $\lambda = 0.05$. One-undulation case. ϕ increasing from (a) 0° to (l) 330° in steps of 30°.

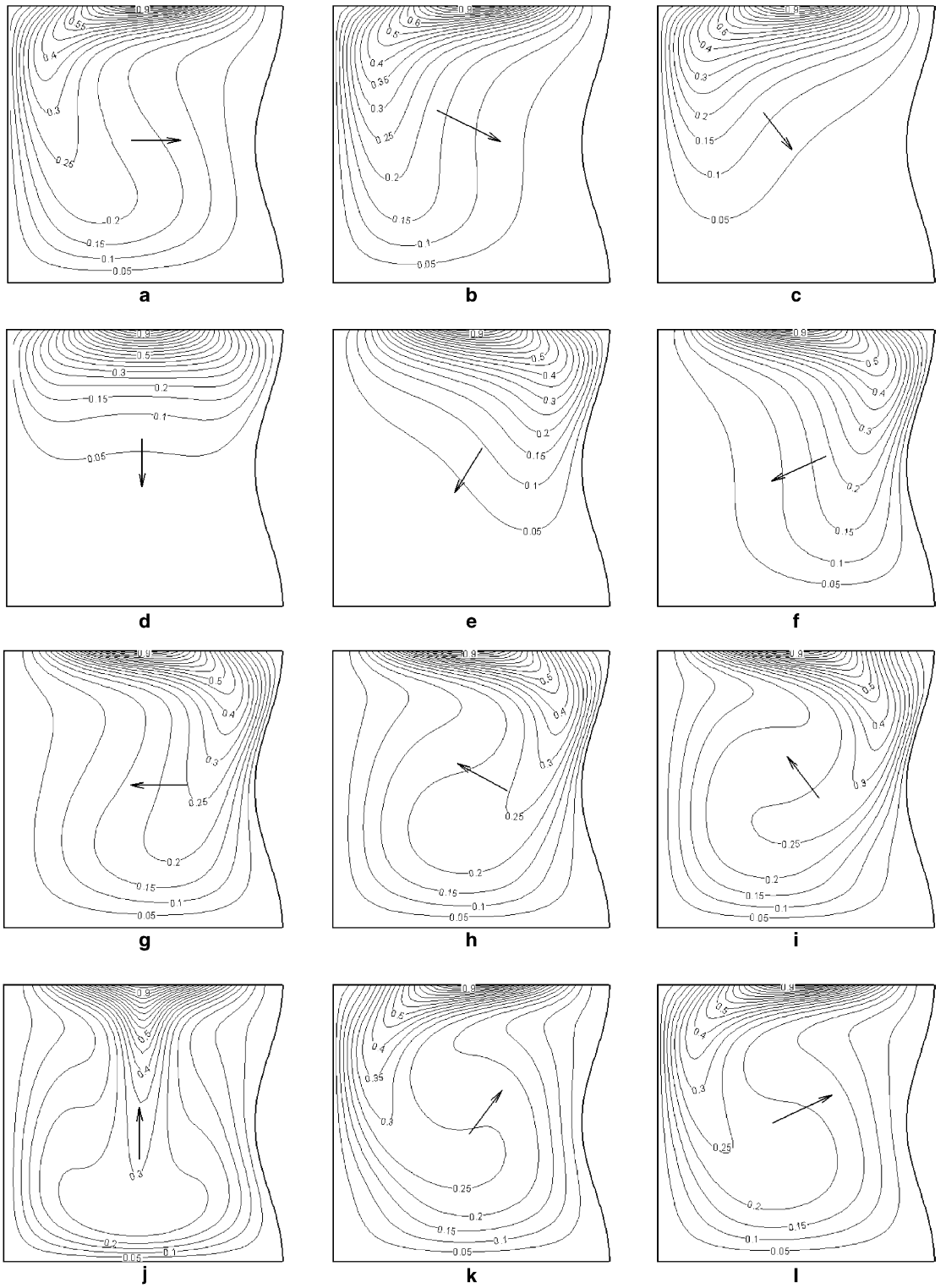

Fig. 6. Isotherms for $Ra = 10^5$, $\lambda = 0.05$. One-undulation case. ϕ increasing from (a) 0° to (l) 330° in steps of 30°.

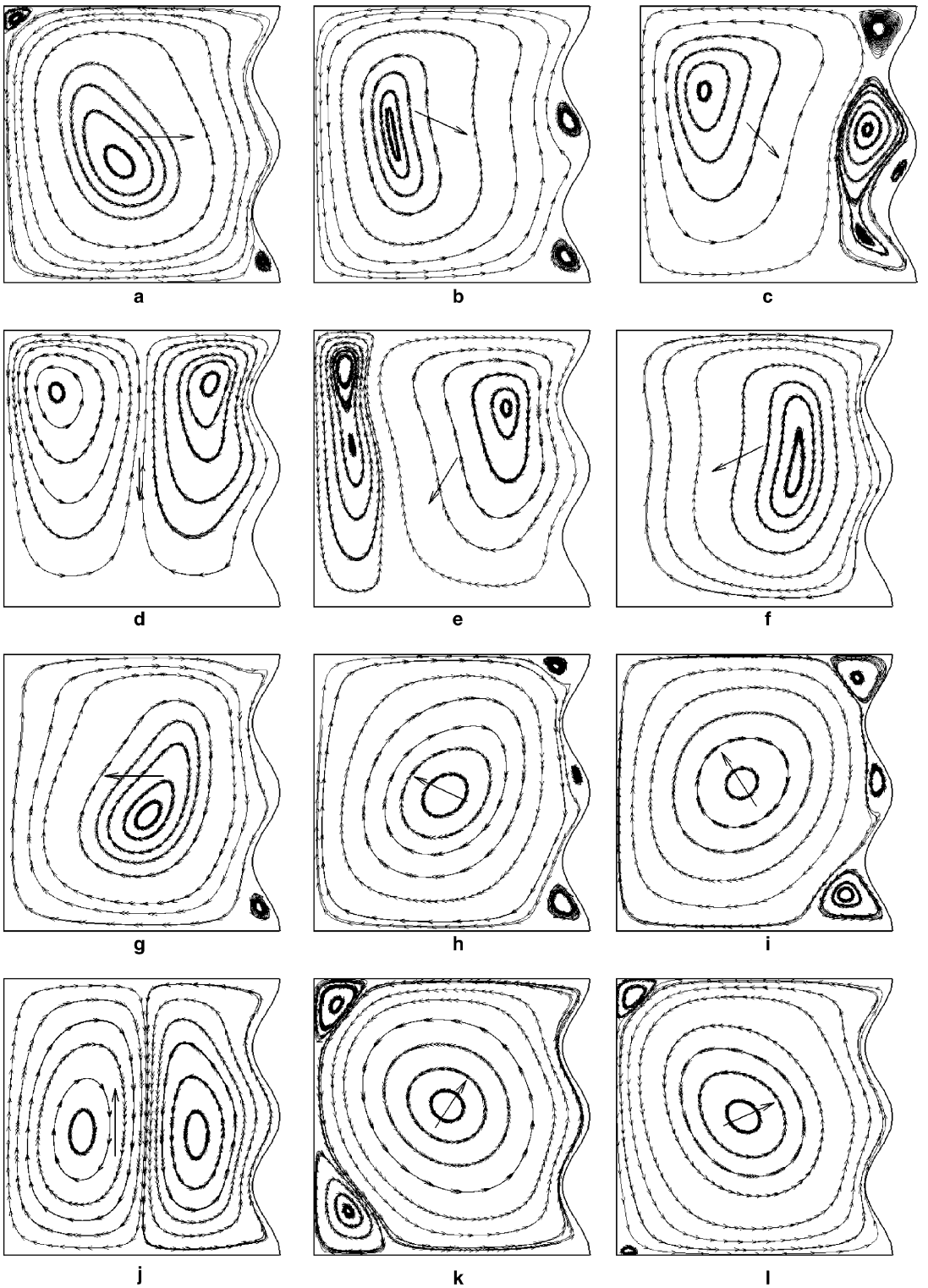

Fig. 7. Streamtraces for $Ra = 10^5$, $\lambda = 0.05$. Two-undulation case. ϕ increasing from (a) 0° to (l) 330° in steps of 30°.

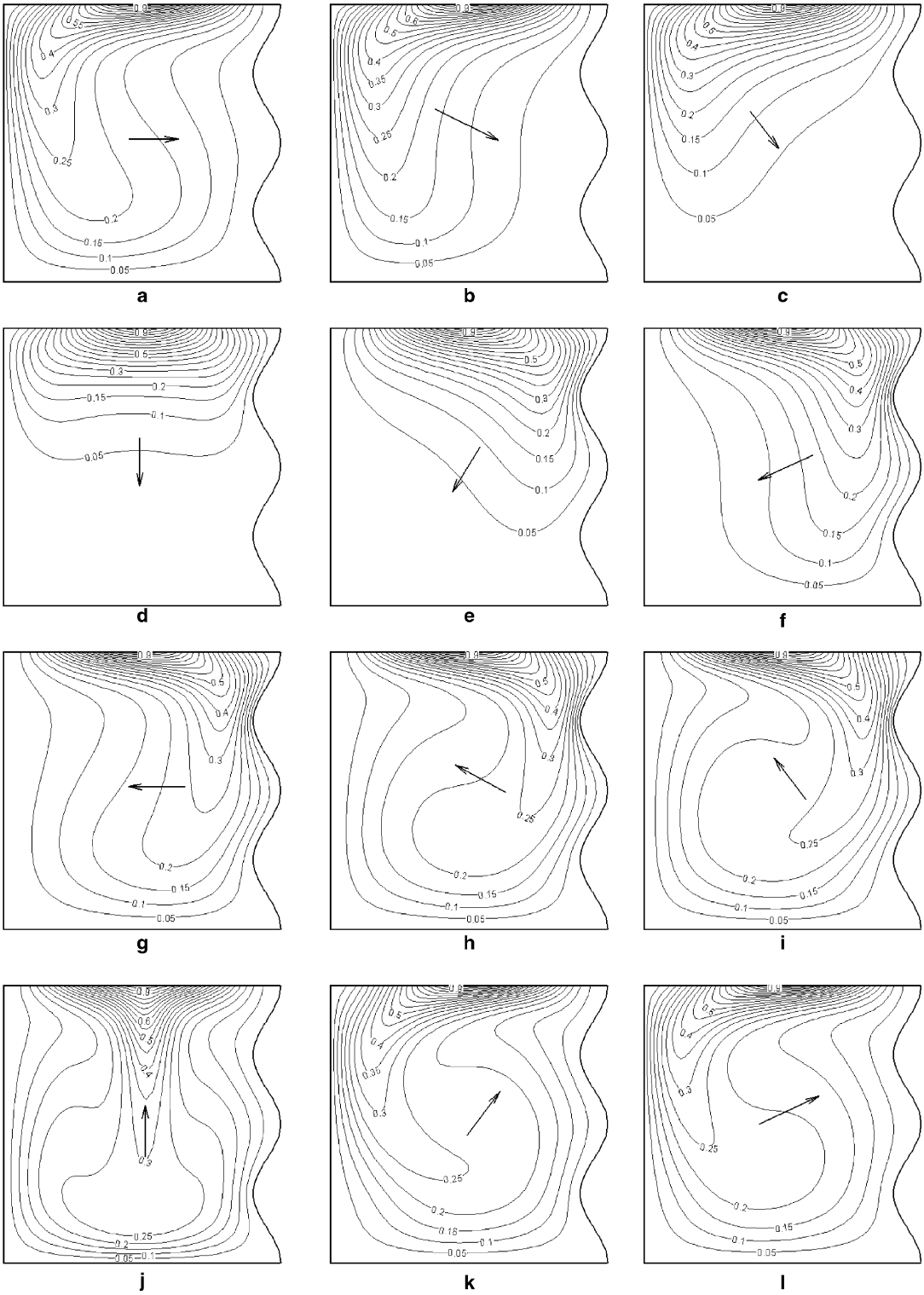

Fig. 8. Isotherms for $Ra = 10^5$, $\lambda = 0.05$. Two-undulation case. ϕ increasing from (a) 0° to (l) 330° in steps of 30°.

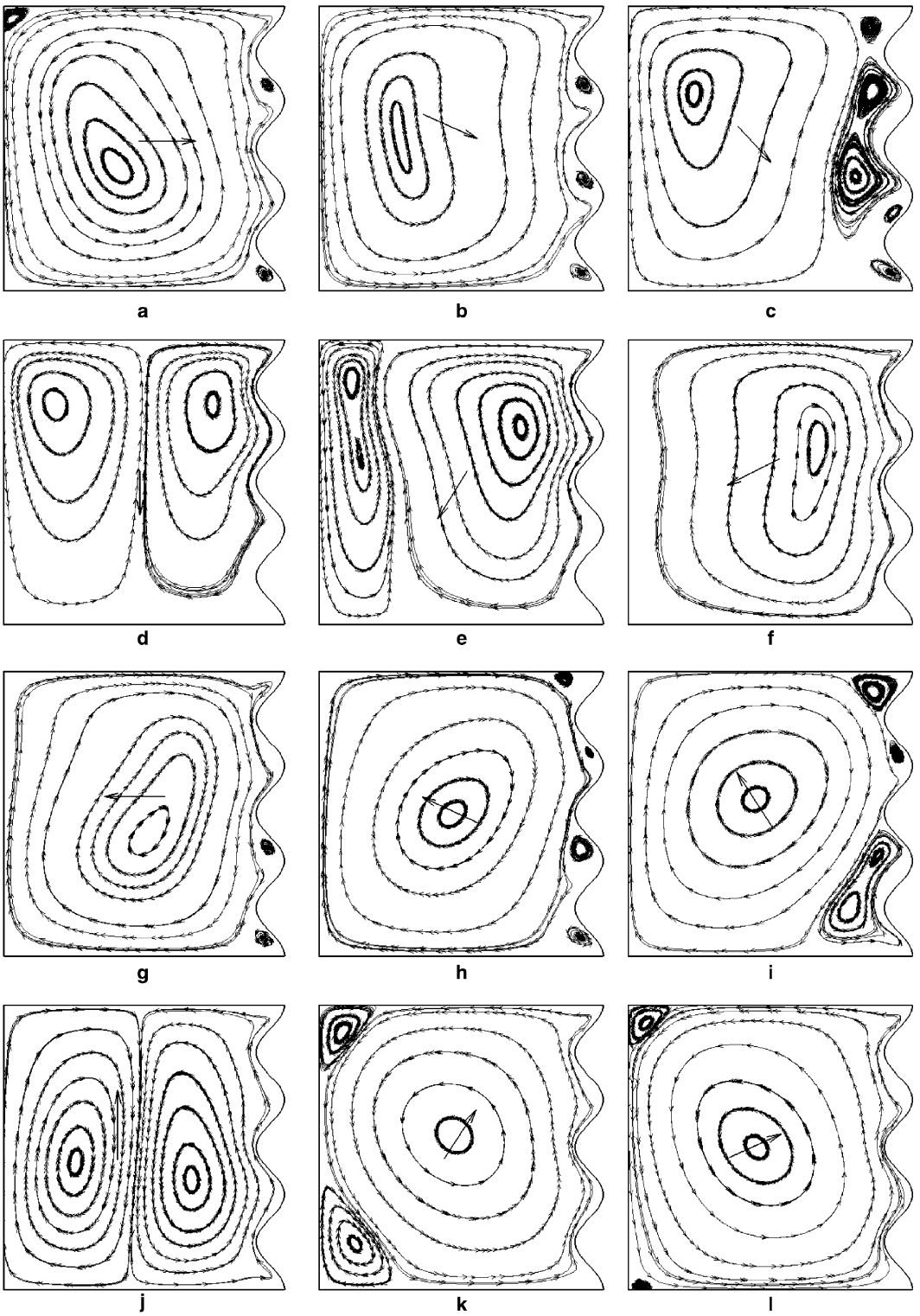

Fig. 9. Streamtraces for $Ra = 10^5$, $\lambda = 0.05$. Three-undulation case. ϕ increasing from (a) 0° to (l) 330° in steps of 30°.

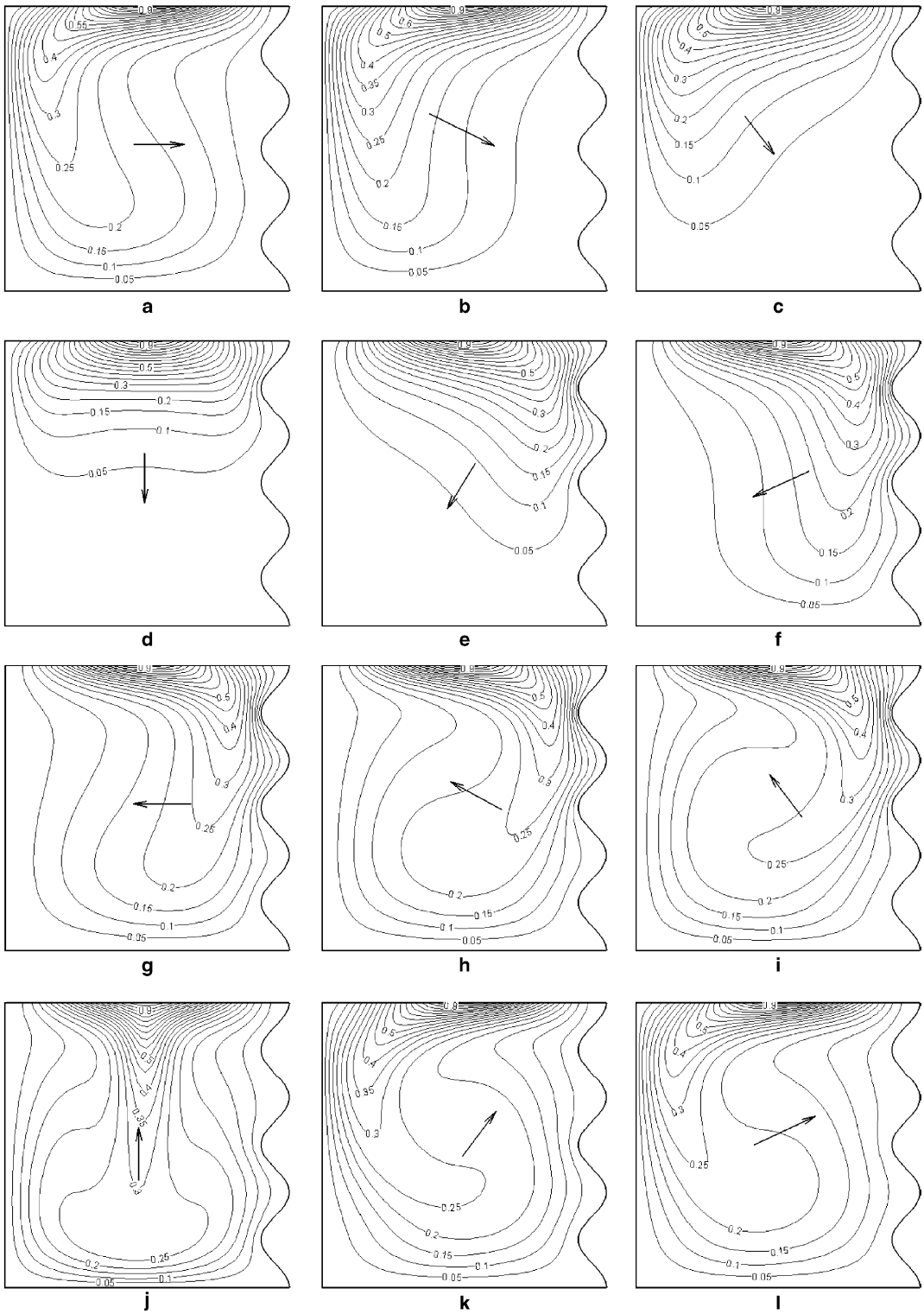

Fig. 10. Isotherms for $Ra = 10^5$, $\lambda = 0.05$. Three-undulation case. ϕ increasing from (a) 0° to (l) 330° in steps of 30°.

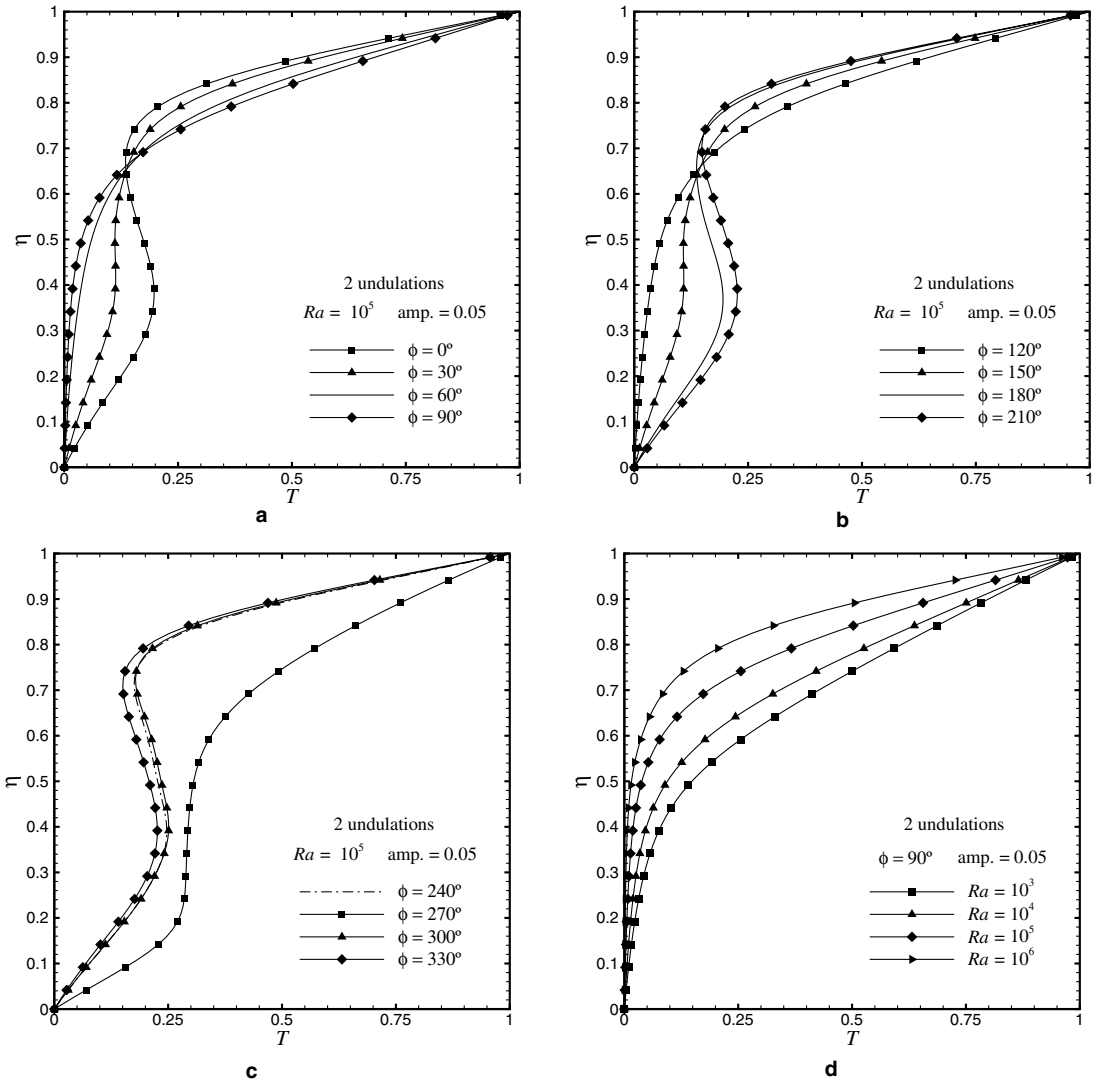

Fig. 11. Temperature distribution at $x = 0.5$ along vertical line for different ϕ.

layer thickness decreases because T attains bottom wall temperature value in a shorter distance from the top wall.

4.3. Nusselt number

4.3.1. Average Nusselt number (Nu_{av})

The variations of Nu_{av} with ϕ for the wavy wall are plotted in Fig. 12(a)–(c). With amplitude 0.05 and $Ra = 10^5$, Nu_{av} decrease, then increase and finally decrease with the increase of ϕ for one-, two- and three-undulations (Fig. 12(a)). The negative sign implies that heat is transferred from the domain to the surroundings. It is observed that the number of undulations does not have appreciable effect on Nu_{av}. Fig. 12(b) and (c) give the plot for amplitude 0.025 and 0.05 for one-undulation and three-undulations, respectively. In both cases, the amplitude does not have any appreciable effect on Nu_{av}. In all the three cases (Fig. 12(a)–(c)), it is observed that the minimum occurs for $\phi = 30°$ and the maximum occurs for $\phi = 180°$. Also to be noted that there is a valley spreading for $\phi \approx 150°$–$240°$ (in all the cases) for which the Nu_{av} remains approximately same. This is due to the similar isotherm patterns as shown in Fig. 6(f)–(i), Fig. 8(f)–(i), Fig. 10(f)–(i).

The Nu_{av} vs wave amplitude (λ) are shown in Fig. 13(a)–(c) for various Ra and undulations when $\phi = 90°$. For $\lambda = 0$, there is no undulation. Nu_{av} value is same for $Ra = 10^2$–10^4 (Fig. 13(a)–(c)). It increases for $Ra = 10^5$ and 10^6. This is happening because conduction

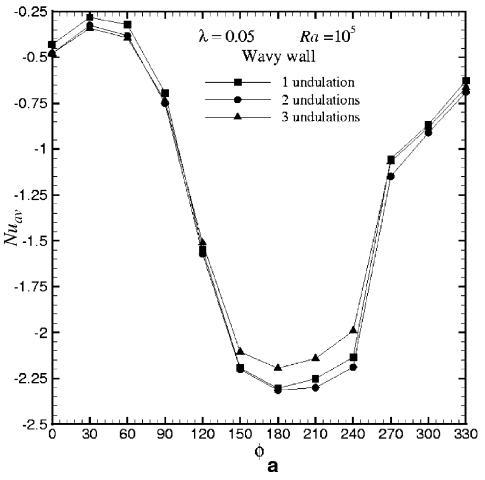

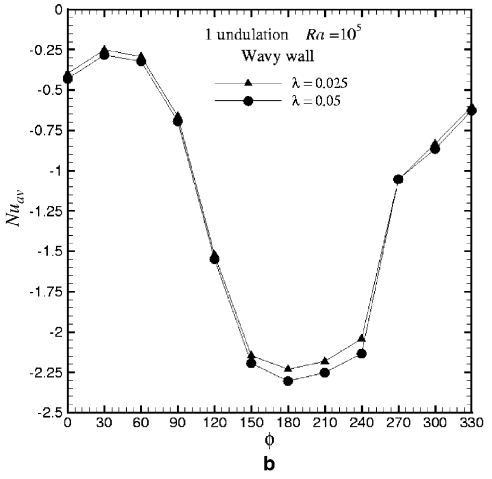

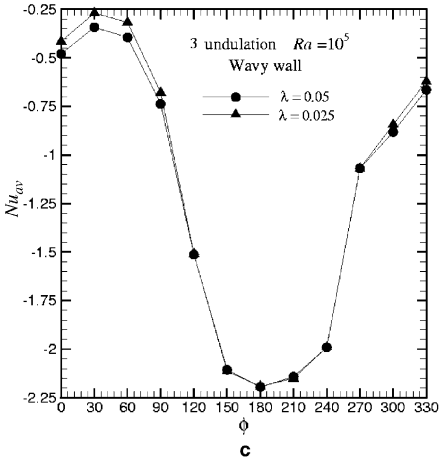

Fig. 12. Average Nusselt number (Nu_{av}) vs ϕ.

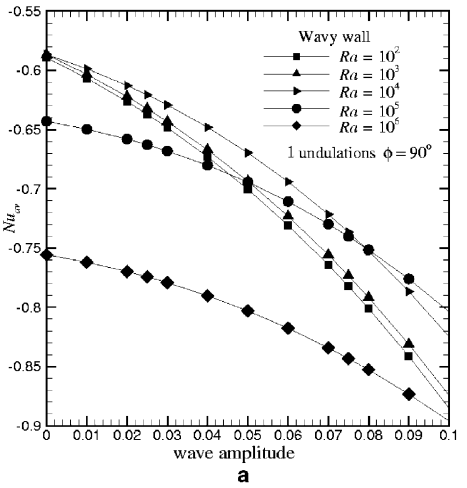

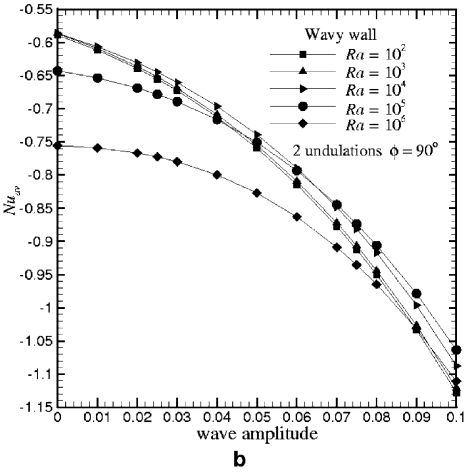

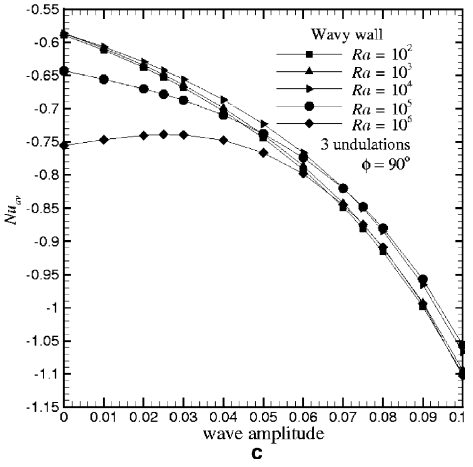

Fig. 13. Average Nusselt number (Nu_{av}) vs wave amplitude (λ).

is the mode of heat transfer for Ra up to 10^4 whereas advection mode of heat transfer starts dominating with increase of $Ra = 10^5$–10^6. This results in the increase of Nu_{av}. This limit of Ra is exactly matching with the results of Sarris et al. [12]. For one-undulation case (Fig. 13(a)), Nu_{av} increases with wave amplitude for $Ra = 10^2$–10^6. In

the range $Ra = 10^2$–10^4, the gain in Nu_{av} decreases with the increase in Ra. The Nu_{av} variation for $Ra = 10^5$ and 10^6 is different than those of 10^2–10^4. At high Ra the advection mode of heat transfer is affected by the waviness of wall. Also there is a change of flow pattern. A typical flow pattern at $Ra = 10^6$, $\lambda = 0.1$ and $\phi = 90°$ is shown in Fig. 14(a)–(c) for one-, two- and three-undulations. The core of the cell adjacent to the wavy wall is breaking into two smaller cells. This behaviour starts at $Ra = 10^5$ and more pronounced in the case of $Ra = 10^6$ and with higher amplitude. Similar type of change of flow pattern due to the presence of non-rectangular wall at $Ra = 10^5$ and above has been reported by Oosthuizen and Monaghan [24]. The corresponding isotherms are shown in Fig. 14(d) and (e). This may be the reason why Nu_{av} is decreasing with increase in λ.

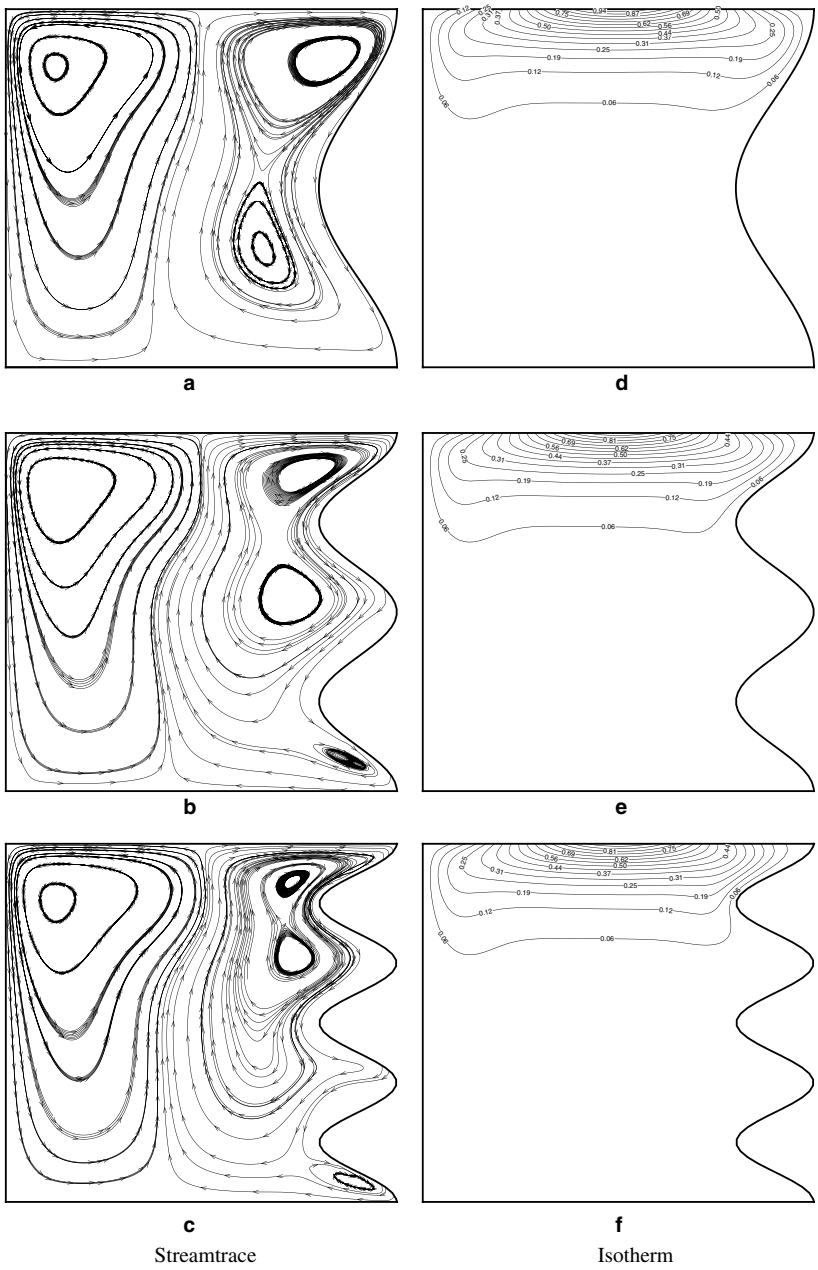

Fig. 14. Streamtrace and isotherm plots for $Ra = 10^6$, $\lambda = 0.1$ and $\phi = 90°$.

4.3.1.1. Number of undulations. The variation of Nu_{av} with wave amplitude for various number of undulations are given in Fig. 15(a)–(d) for $Ra = 10^3$, 10^4, 10^5 and 10^6, respectively. For all the cases, Nu_{av} increases from one-undulation to two-undulations. However with further increase from two- to three-undulations, Nu_{av} decreases. This is due to the fact that three-undulation case is making the fluid to separate out at the bottom undulation and thus opposing the heat transfer. Thus increasing the number of undulations from two to three has detrimental effect as far as heat transfer is concerned. The Nu_{av} values for two- and three-undulations are less than the one-undulation case for $\lambda = 0$–0.026 and 0–0.066, respectively, when $Ra = 10^6$ (Fig. 15(d)). It has been observed that the right side primary cell breaks into two smaller vortices when Ra is increased from 10^5 to 10^6 (Fig. 14(a)–(c)). This may be the reason for this different behaviour.

4.3.1.2. Effect of amplitude (λ). When the amplitude is zero (i.e., a square cavity without undulation), Nu_{av} on the undulated wall is constant up to $Ra = 10^4$ (conduction mode) and then increases with increase in Ra (convection mode) (Fig. 16(a)–(c)). It is noticed that with a finite amplitude, Nu_{av} decreases as the advection mode starts playing a role. It then increases with further increase of Ra giving rise to a local minima. This may be due to the complex fluid-wavy wall interaction. It is also to be noted that with increase in amplitude, the range of Ra for which Nu_{av} is constant (conduction) decreases. The result is that even with small Ra, Nu_{av} is high if λ is high. Effective heat transfer rate can be increased with low Ra (the buoyancy effect is small). For two-undulations (Fig. 16(b)), similar trend is observed and the magnitude of Nu_{av} is more. However, the magnitude decreases for three-undulations (Fig. 16(c)) and earlier described in Fig. 15.

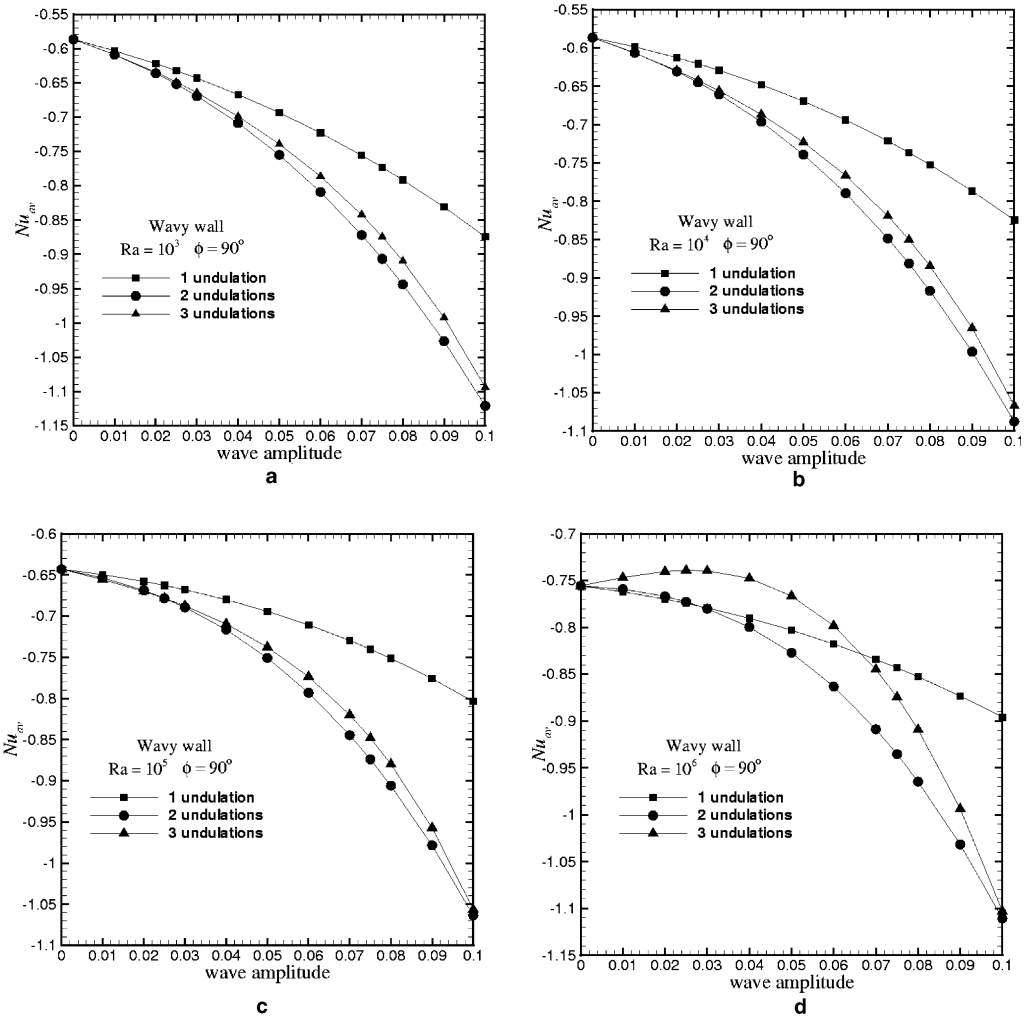

Fig. 15. Average Nusselt number distribution with λ.

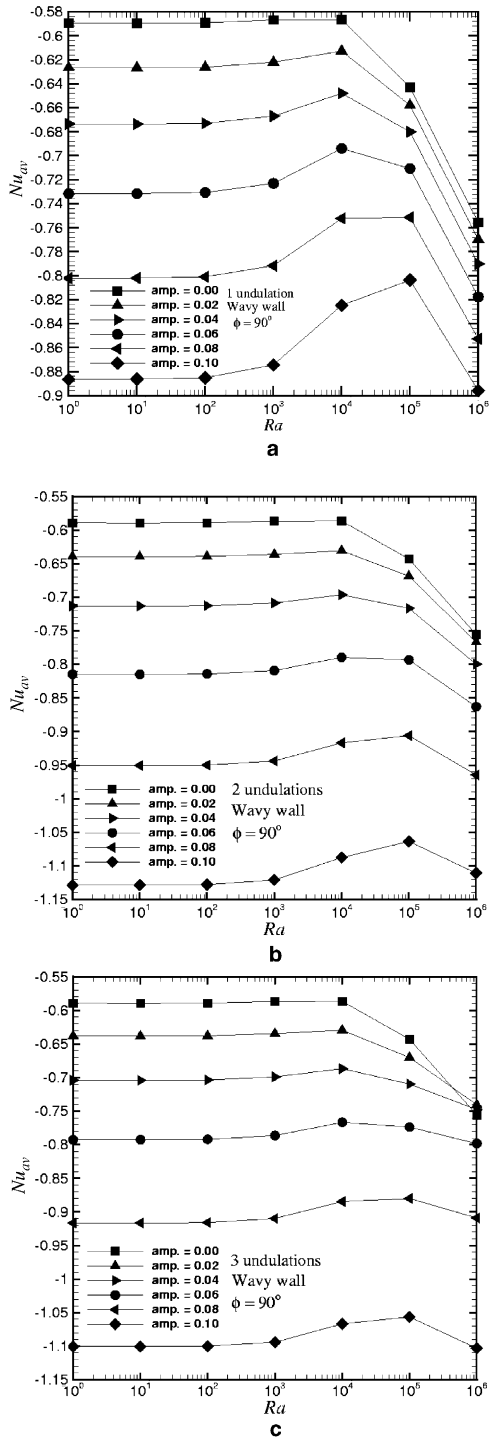

Fig. 16. Average Nusselt number distribution for different amplitude.

4.3.1.3. Top heated wall. The heat coming into the domain is dissipated by the three cold walls. So the Nu_{av} on this wall is an indication of the amount of heat transfer through the domain. The variation of Nu_{av} for the heated wall with inclination angle is shown in Fig. 17(a) for amplitude 0.05, $Ra = 10^5$ and three different number of undulations. It is observed that Nu_{av} is decreasing in the range 0°–90° from nearly 3.5 to a little less that 1.5. It is then increasing to 4.5 up to an angle 270° and finally decreasing to the value at 0°. The distribution lines are practically overlapping for one-, two- and three-undulations. There is a distinct minimum and maximum locations obtained corresponding to 90° and 270°, respectively. This is due to the abrupt change in the isotherm patterns as shown in Figs. 6, 8 and 10.

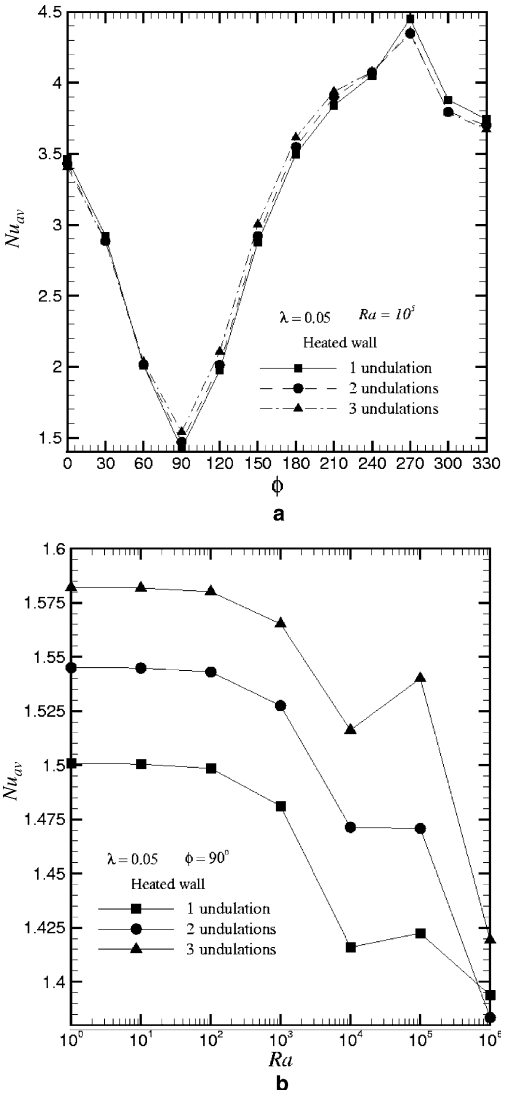

Fig. 17. Average Nusselt number distribution for the heated wall. Variation of Nu_{av} with (a) different inclination angle and (b) different Ra.

Fig. 17(b) shows the variation of Nu_{av} with Ra for amplitude = 0.05, $\phi = 90°$. With increase in Ra, there is a drop of Nu_{av} by 10% for two- and three-undulations and 7% for one-undulation. This drop may possibly be attributed to the fluid flow structure which adversely affects the heat dissipation from three cold surfaces.

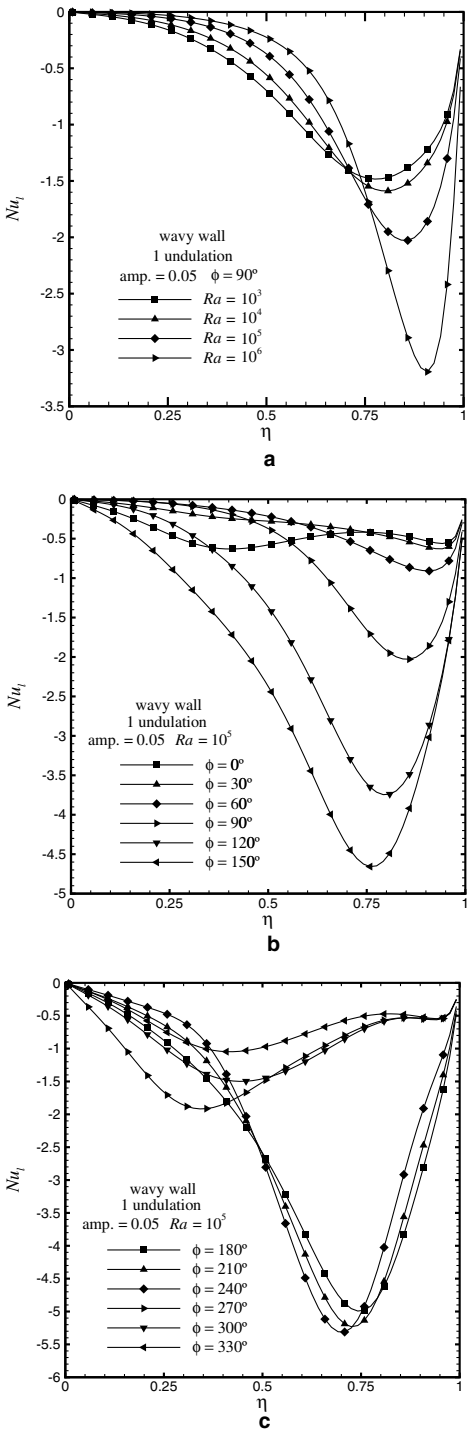

Fig. 18. Local Nusselt number distribution for one-undulation.

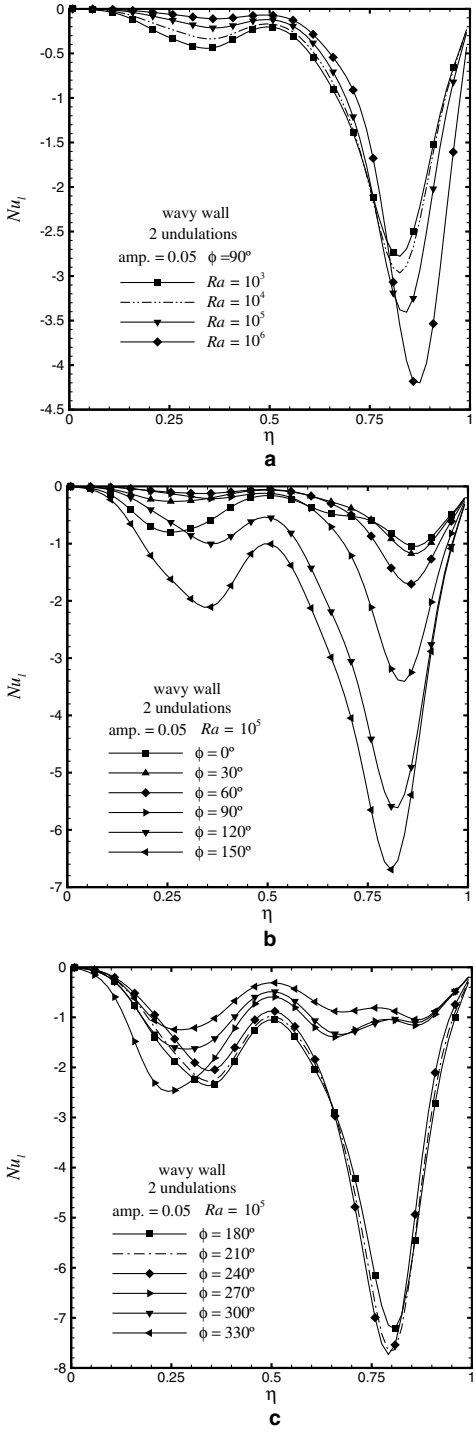

Fig. 19. Local Nusselt number distribution for two-undulations.

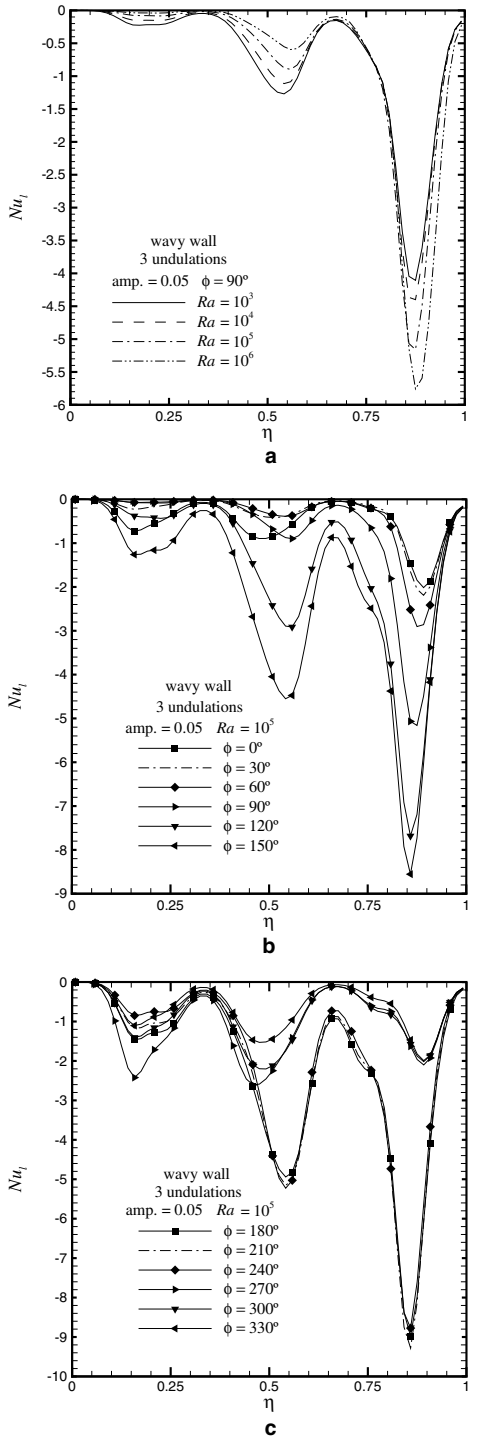

Fig. 20. Local Nusselt number distribution for three-undulations.

4.3.2. Local Nusselt number (Nu_l) distribution

4.3.2.1. Effect of Ra. Nu_l vs η distributions for various *Ra* are shown in Fig. 18(a), Fig. 19(a) and Fig. 20(a) for one-, two- and three-undulations, respectively. With the increase of *Ra*, the maximum Nu_l is increasing near the top (Fig. 18(a)) whereas it is decreasing near the bottom portion of the wavy wall. As the advection dominates with high *Ra*, Nu_l increases at the top portion of the wavy wall. At the same time fluid velocity is high and it gets deflected from the crest of the wall and thus at the bottom portion, there is not much fluid circulation and Nu_l decreases. For two-undulations, there are two maxima for Nu_l and for three-undulations, there are three maxima. The point to be noted is that at the uppermost undulation, the largest *Ra* has the highest Nu_l value whereas for bottom undulation, it has the lowest Nu_l value which is in accordance with the above justification.

4.3.2.2. Effect of ϕ. The variation of Nu_l with ϕ at step of 30° are shown in Fig. 18(b)–(c), Fig. 19(b)–(c) and Fig. 20(b)–(c). The Nu_l distribution value are consistently very close to each other in the range $\phi = 150°$–240°. This is due to the similar isotherm pattern in this range (refer Section 4.1). They are appreciably higher also compared to those values at other angles of variation. This is the reason why the Nu_{av} values are close to each other in this range (Fig. 12).

5. Conclusions

In this study, numerical results of natural convection heat transfer in a two-dimensional enclosure subjected to steady sinusoidal temperature boundary condition on one wall and constant temperature on other three walls are presented. One of the constant-temperature wall is curved having undulation. The number of the undulations has been varied from one to three. The influence of amplitude, *Ra*, angle (ϕ) on the flow patterns and heat transfer characteristics in the enclosure is examined in detail. From the results presented above, the following main conclusions may be drawn.

- With the orientation angle (ϕ), one convection cell gradually transforms into two counter rotating cells for all the undulation cases.
- For $\phi = 90°$, the temperature profile at $x = 0.5$ resembles a boundary layer profile. The boundary layer thickness reduces with increase in *Ra*. For other angles, the shape of the profile depends upon the convection strength.
- For all the type of undulation, maximum Nu_{av} for the wavy wall occurs in the range $\phi = 150°$–240° and minimum Nu_{av} occurs at $\phi = 30°$.
- For all finite amplitude, Nu_{av} shows a minimum for the range of *Ra* studied.
- For small *Ra*, it is possible to increase Nu_{av} on the wavy wall with increase of amplitude.

- With high Ra and large amplitude, the cell near the wavy wall shows a different flow pattern.
- With increase in Ra, Nu_{av} on the wavy wall decreases with increase in amplitude.
- With increase in amplitude, the heat transfer on the wavy wall decreases for three-undulations case compared to one- and two-undulations cases.
- Local Nu_l on the wavy wall has higher value for ϕ = 150°–240° compared to other angles of inclination.

Acknowledgements

The helpful comments by the reviewers are gratefully acknowledged by the authors.

References

[1] S. Ostrach, Natural convection in enclosures, J. Heat Transfer 110 (4-B) (1988) 1175–1190.
[2] S. Noorshahi, C. Hall, E. Glakpe, Effect of mixed boundary conditions on natural convection in an enclosure with a corrugated surface, in: ASME-JSES-KSES International Solar Energy Conference Part 1 (of 2), Maui, HI, April 5–9, 1992, pp. 173–181.
[3] M.R. Amin, Natural convection heat transfer in enclosures fitted with a periodic array of hot roughness elements at the bottom, Int. J. Heat Mass Transfer 36 (3) (1993) 755–763.
[4] L.S. Yao, Natural convection along a vertical wavy surface, J. Heat Transfer 105 (August) (1983) 465–468.
[5] L. Adjlout, O. Imine, A. Azzi, M. Belkadi, Laminar natural convection in an inclined cavity with a wavy wall, Int. J. Heat Mass Transfer 45 (2002) 2141–2152.
[6] P. Chao, H. Ozoe, S.W. Churchill, Effect of a non-uniform surface temperature on laminar natural convection in a rectangular enclosure, Chem. Eng. Commun. 9 (1–6) (1981) 245–254.
[7] P.K.-B. Chao, H. Ozoe, S.W. Churchill, N. Lior, Laminar natural convection in an inclined rectangular box with the lower surface half-heated and half-insulated, J. Heat Transfer 105 (3) (1983) 425–432.
[8] W.-S. Fu, C.-C. Tseng, Y.-C. Chen, Natural convection in an enclosure with non-uniform wall temperature, Int. Commun. Heat Mass Transfer 21 (6) (1994) 819–828.
[9] V. Shukla, R. Murtugudde, V. Prasad, M. Cane, Natural convection in a horizontal cavity with a linear temperature variation on the top, in: 27th National Heat Transfer Conference, Mixed Convection Heat Transfer, ASME HTD, vol. 163, 1991, Minneapolis, pp. 1–8.
[10] P.H. Oosthuizen, J.T. Paul, Free convection in a square cavity with a partially heated wall and a cooled top, J. Thermophys. Heat Transfer 5 (4) (1991) 583–588.
[11] P.H. Oosthuizen, Free convective flow in an enclosure with a cooled inclined upper surface, Comput. Mech. 14 (5) (1994) 420–430.
[12] I.E. Sarris, I. Lekakis, N.S. Vlachos, Natural convection in a 2D enclosure with sinusoidal upper wall temperature, Numer. Heat Transfer, Part A 42 (2002) 513–530.
[13] C.R. Maliska, G.D. Raithby, A method for computing three dimensional flows using non-orthogonal boundary-fitted co-ordinates, Int. J. Numer. Meth. Fluids 4 (1984) 519–537.
[14] C.R. Maliska, F.E. Milioli, A non-orthogonal model for the solutions of natural convection problems in arbitrary cavities, in: C. Taylor, P.M. Gresho, Habashi, M.D. Olson (Eds.), 3rd International Conference in Numerical in Laminar and Turbulent Flow, 1985, pp. 805–816.
[15] J.F. Thompson, Z.U.A. Warsi, C.W. Mastin, Numerical Grid Generation, North Holland, 1985, pp. 188–235.
[16] M.N. Özisik, Finite Difference Methods in Heat Transfer, CRC Press, London, 1994, pp. 307–353.
[17] S.V. Patankar, Numerical Heat Transfer and Fluid Flow, Hemisphere Publishing Co., New York, 1980, pp. 113–147.
[18] T. Hayase, J.C. Humphrey, R. Greif, A consistently formulated quick scheme for fast and stable convergence using finite-volume iterative calculation procedures, J. Comput. Phys. 98 (1992) 118–180.
[19] H.K. Versteeg, W. Malalasekera, An Introduction to Computational Fluid Dynamics, the Finite Volume Method, Longman Group Ltd., Malaysia, 1995.
[20] J.P. Van Doormaal, G.D. Raithby, Enhancements of the simple method for predicting incompressible fluid flows, Numer. Heat Transfer 7 (1984) 147–163.
[21] G. de Vahl Davis, Natural convection of air in a square cavity: a benchmark numerical solution, Int. J. Numer. Meth. Fluids 3 (1983) 249–264.
[22] N.C. Markatos, K.A. Perikleous, Laminar and turbulent natural convection in an enclosed cavity, Int. J. Heat Mass Transfer 27 (5) (1984) 755–772.
[23] G.V. Hadjisophocleous, A.C.M. Sousa, J.E.S. Venart, Prediction of transient natural convection in enclosures of arbitrary geometry using a nonorthogonal numerical model, Numer. Heat Transfer 13 (1988) 373–392.
[24] P.H. Oosthuizen, P.F. Monaghan, Free convective flow in a vertical non-rectangular cavity with a cooled flat upper surface, in: Natural/Forced Convection and Combustion Simulation, 1992, pp. 191–208.